Final report

Project Title: Catalytic production of ethanol from biomass-derived synthesis gas
DOE Award Number: 3.3.2.6

Recipient: Prof. Victor S.-Y. Lin (PI) and Prof. Robert C. Brown (co-PI)
Project Location: Iowa State University

Reporting Period: July 2008 – July 2012
Date of Report June, 2016
Written by: Brian Trewyn and Ryan Smith

Executive summary: Heterogeneous catalysts have been developed for the conversion of biomass-derived synthetic gas (syngas) to ethanol. The objectives of this project were to develop a clean synthesis gas from biomass and develop robust catalysts with high selectivity and lifetime for C_2 oxygenate production from biomass-derived syngas and surrogate syngas. During the timeframe for this project, we have made research progress on the four tasks: (1) Produce clean bio-oil generated from biomass, such as corn stover or switchgrass, by using fast pyrolysis system, (2) Produce clean, high pressure synthetic gas (syngas: carbon monoxide, CO, and hydrogen, H_2) from bio-oil generated from biomass by gasification, (3) Develop and characterize mesoporous mixed oxide-supported metal catalysts for the selective production of ethanol and other alcohols, such as butanol, from synthesis gas, and (4) Design and build a laboratory scale synthesis gas to ethanol reactor system evaluation of the process. In this final report, detailed explanations of the research challenges associated with this project are given. Progress of the syngas production from various biomass feedstocks and catalyst synthesis for upgrading the syngas to C_2-oxygenates is included. Reaction properties of the catalyst systems under different reaction conditions and different reactor set-ups are also presented and discussed. Specifically, the development and application of mesoporous silica and mesoporous carbon supports with rhodium nanoparticle catalysts and rhodium nanoparticle with manganese catalysts are described along with the significant material characterizations we completed. In addition to the synthesis and characterization, we described the activity and selectivity of catalysts in our micro-tubular reactor (small scale) and fixed bed reactor (larger scale). After years of hard work, we are proud of the work done on this project, and do believe that this work will provide a solid foundation for the future production of syngas from biomass and the development of heterogeneous catalysts for the syngas to C_2-oxygenate process and for the commercialization of this process.

Below is the original project management program, which outlines the goals and milestones affiliated with this project.

A. Efficient conversion of switchgrass to synthesis gas

A.1. Production of clean bio-oil from switchgrass by using existing fast pyrolysis system at ISU

- A.1.1. Production of bio-oil from switchgrass
  - A.1.1.ML.1 Optimized system operating conditions for producing bio-oil obtained. **C**
- A.1.2. Characterization of bio-oil produced from switchgrass
  - A.1.2.ML.1 Complete physical and chemical characterizations of bio-oil for evaluating their qualities were completed. **C**

A.2. Design and construction of high-pressure bio-oil gasification system

- A.2.1. Planning and design of high pressure bio-oil gasification system
  - A.2.1.ML.1 Detailed design drawings complete; equipment and materials ordered.
- A.2.2. Construction of high pressure bio-oil gasification system
  - A.2.2.ML.1 Gasification system is fully installed and operational for shake down tests
- A.2.3. Characterization of bio-oil produced from switchgrass in high pressure bio-oil gasification system
  - A.2.3.ML.1 Complete physical and chemical characterization of bio-oil for evaluating their qualities is completed.
- A.2.4 Shake down trials.
  - A.2.4.ML.1 Continuous uninterrupted eight hour bio-oil gasification using switchgrass bio-oil

A.3 Production of clean synthesis gas from bio-oil

- A.3.1. Production of synthesis gas using non-catalytic gasification mode
  - A.3.1.ML.1 Optimized operating conditions for non-catalytically converting bio-oil to synthesis gas obtained.
- A.3.2 Production of synthesis gas from bio-oil using catalytic gasification mode
  - A.3.2.ML.1 Catalytic production of synthesis gas from bio-oil is demonstrated and evaluated.

B. Selective C_2-oxygenation catalyst for converting synthesis gas to ethanol

B.1. Identify a robust catalyst with high selectivity, long lifetime, and high per-pass conversion for the production of ethanol

- B.1.1. Complete analysis of identified catalyst for conversion of synthesis gas to ethanol

B.2. Identify and synthesize a Lewis acid promoter/catalyst support that works best with the previously determined catalyst

- B.2.1. Compare candidates (Mn, Li, Zr, etc) to determine best promoter to work in a symbiotic fashion with the catalyst
- B.2.2. Synthesize mesoporous promoter/catalyst support without phase separation
  - B.2.2.ML.1. Total synthesis of single phase catalyst support with Lewis acid promoter evenly distributed in the framework

C. Characterization of synthesis gas catalysts

C.1. Full characterization of functional groups inside the pores with high resolution and sensitivity

- C.1.1. Measure the degree of functionalization of the support with determined catalyst
- C.1.2. Study the structure and conformation of all surface species in the catalysts
- C.1.3. Estimate the overall catalyst loading
    - C.1.ML.1. Total characterization of catalyst support including degree of functionalization and catalyst loading

C.2. Fully characterization of supported catalytic metal particles

- C.2.1. Determine the dispersion of catalytic metal particles and the ratio between catalyst and promoter
- C.2.2. Demonstrate the cooperative nature of the catalysts

D. Demonstration of synthesis gas to ethanol reaction

D.1. Design and build a laboratory scale synthesis gas to ethanol reactor system

- D.1.1. Design laboratory scale synthesis gas to ethanol reactor system
- D.1.2. Build a laboratory scale synthesis gas to ethanol reactor system

D.2. Establish the communication between the gas mass flow controllers with the data acquisition system

D.3. Develop a standard operating procedure to ensure safe operation

D.4. Actual testing of the catalysts of total conversion of synthesis gas to ethanol

- D.4.ML.1 Continuous uninterrupted bio-oil gasification to ethanol using switchgrass bio-oil and catalyst.

During the timeframe of this project we made substantial progress on both individual research fronts. Getting syngas from bio-oil proved to be a challenging research endeavor. These challenges and achievements are outlined here.

1. The first objectives set by CSET was to produce bio-oil from switchgrass via fractionalization of the feedstock and collect and characterize the fractions. This was accomplished by utilizing an existing pyrolysis reactor CSET had previously built and tested, shown in **Figure 1**. The schematic in Figure 1 shows the unit operating with four stage fractions. However, the pyrolysis trials with oak were performed with five stage fractions, as an additional condenser was used at the end of the collection train. Switchgrass trials included a sixth stage fraction, which was an electrostatic precipitator (ESP). Properties of the bio-oil fractions collected from oak wood are outlined in **Table 1**. We determined that the chemical components in bio-oil are distributed differently among the bio-oil fractions. Light MW components are concentrated in fraction 5, while the heavier components are concentrated in fractions 1 and 2. The first studies were completed on oak wood, mainly because that is what we had available and could use these results as a base line for our product distribution of switchgrass. Bio-oil properties divided into fractions is outlined in **Table 2.**

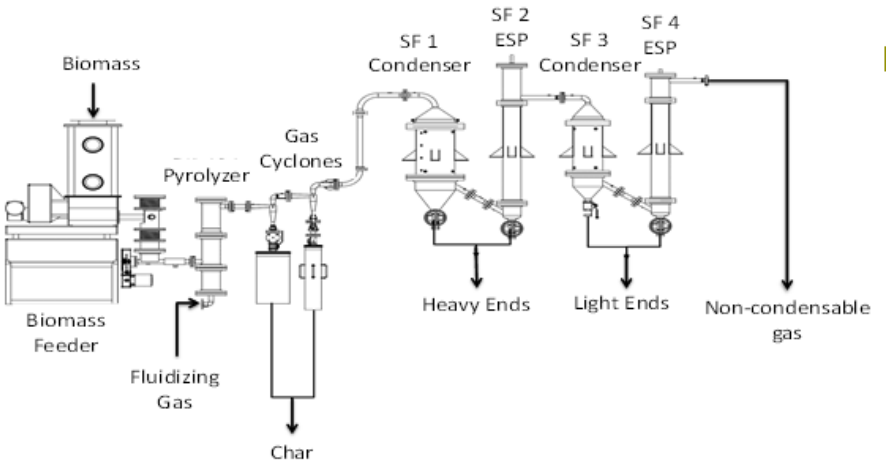

Figure 1. Schematic diagram of the 8 kg/h fast pyrolysis reactor with staged bio-oil collection unit.

Characterizing the fractions from the fast pyrolysis of oak wood and switchgrass allowed us to compare the pyrolysis of a known feedstock to a new feedstock. As can be seen by comparing the table there was considerably more moisture in the switchgrass than the oak wood that showed up in later fractions.

Table 1. Properties of bio-oil fractions collected from fast pyrolysis of oak wood using ISU fast pyrolysis system.

Analysis of Bio-oil Fractions Produced from Fast Pyrolysis of Oak wood										
Fraction #	Moisture Content (wt%)	Total Acid Number (TAN)	Analysis by TGA (wt%)		Water Insolubles (wt%)	Elemental Composition (with water)				HHV (MJ/kg)
			Fixed Carbon	Ash		%C	%H	%N	%O*	
1	2.58	36.9	32.16	0.84	49.15	59.1	6.1	0.34	34.5	23.28
2	6.62	42.3	29.08	Nil	40.93	58.6	6.4	0.15	34.8	23.52
3	4.67	57.7	20.44	Nil	20.03	52.2	6.7	0.14	41.0	20.89
4	7.76	84.6	22.64	0.41	28.85	50.6	6.6	0.10	42.7	19.94
5	53.38	133.6	2.74	0.23	0.32	19.2	9.0	0.01	71.8	8.17
Whole Bio-Oil	29.35	70.1	12.9	0.02	18.62	38.3	7.8	0.02	53.5	15.82

Table 2. Properties of bio-oil fractions collected from fast pyrolysis of switchgrass using ISU fast pyrolysis system.

	Analysis of Bio-oil Fractions Produced from Fast Pyrolysis of Switchgrass											
Fract #	Moisture Content (%wt)	Visco-sity (cst/s)	Total Acid Number	Analysis by TGA (%wt)		Water Insolubles (%wt)	Elemental Composition (w/ water)					HHV (MJ/kg)
				Fixed Carbon	Ash		%C	%H	%N	%S	%O*	
1	5.46	15,282	34.0	29.63	0.46	63.87	61.2	6.5	1.21	0.04	25.9	25.10
2	5.60	889	38.3	26.69	0.46	51.26	61.6	6.8	0.77	0.02	26.6	25.49
3	9.91	779	48.2	22.50	0.18	50.41	56.9	6.9	0.70	0.03	32.1	24.04
4	12.43	20.6	72.5	11.52	0.11	7.59	46.6	7.2	0.26	0.13	44.8	20.27
5	21.52	22.9	126.4	15.89	3.38	5.35	37.7	7.5	0.15	0.12	54.2	15.07
6	76.56	1.0	68.9	0.31	Nil	0.19	10.5	9.3	Nil	0.01	80.0	3.09
whole bio-oil	29.35	35.7	76.1	16.85	0.02	18.62	38.3	7.8	0.02	0.03	53.6	18.02

2. While characterizing the products from switchgrass pyrolysis to determine the optimal bio-oil production conditions, the CSET team began the design and construction of a laboratory-scale reactor for gasifying bio-oil at elevated pressures. Gasification of bio-oil at high pressure has the advantage of producing syngas at high pressure at significantly reduced energy cost compared to the gasification of biomass followed by compression of the syngas product. One challenge associated with this objective is to get the bio-oil to be fed into the reactor chamber as a fine mist. A new bio-oil-air sprayer was designed and manufactured to address this challenge, shown in **Figure 2**. An important factor of this design was for the injected bio-oil to be in intimate contact with oxygen and react quickly with minimum coking. We learned that there are three main parameters for atomization of fluids. The first is the surface tension of the liquid, which affects the amount of force that needs to be applied to shear the fluid to make it exiting the nozzle as atomized droplets. The second parameter is the pressure drop of the air at the exit of the nozzle. The producers of commercially available nozzles suggest to set a pressure drop between 30-50 psi for the exiting air. The third parameter is the angle of attack between

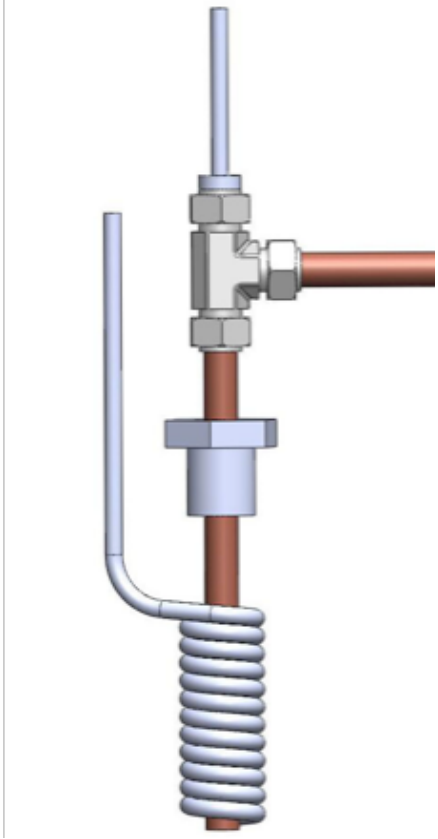

Figure 2. Schematic diagram of the bio-oil-air sprayer for feeding bio-oil/air into the gasifier

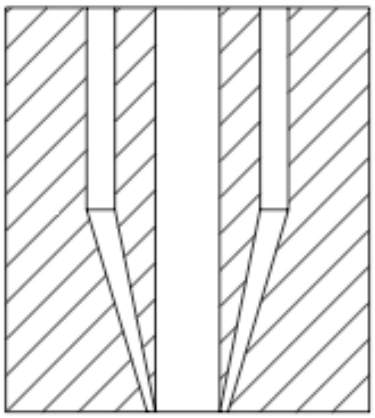

Figure 3: Cross section of the nozzle end.

the air and liquid lines. Changing the angle between the air and liquid the spray angle will increase. By having both the liquid and air exiting in a parallel provides approximately a 15^{o} angle spray from the centerline. The study led to the development of the nozzle shown in **Figure 3**.

To continue the development of the switchgrass derived bio-oil gasifier a test rig was constructed. The construction focused on the assembly and installation of various parts of the system, which included parts for liquid and gas feeding, tubular gasification reactor, particulate removal for gas product cleaning, and gas product analysis. A photograph of the test gasifier rig that operates at atmospheric pressure can be seen in **Figure 4**. The purpose of the atmospheric bio-oil gasification reactor system was to obtain experimental data information on the behavior and operating conditions of bio-oil gasification, which in turn will be used for the design and construction of the high-pressure bio-oil gasification system. This test system allowed us to investigate different parameters that would likely effect the production of syngas. Some of these parameters are outlined below:

- Fuels: Mixture of a commercial bio-oil and methanol
  - Bio-Oil to Methanol ratio (by weight%): 100:0; 75:25; 50:50
  - Bio-oil properties:
    - Elemental composition (wt%, including water): C/H/N/S/O = 38.3/7.8/0.02/0.03/53.6
    - Water content (wt%): 29.35
    - Fixed carbon (wt%): 16.85
    - Ash content (wt%): 0.02
    - Total water insolubles (wt%): 18.62
    - Viscosity (cst): 35.7
    - Total acid number: 76.1
- Reaction temperatures (^{o}C): 700, 800, 900
- Air and fuel flow rates:
  - Air flow rate (L min^{-1}, STP): 2.0, 3.0, 5.0, and 10.0 L min^{-1}
  - Fuel flow rate was varied based on the rate of airflow. Air to fuel ratio was fixed at 25% of theoretical air required for complete fuel combustion.

One significant outcome that was realized was that it will be critically important prevent bio-oil coking during injection into the reactor. A new nozzle design was considered to limit coke formation at the injection nozzle and control temperature by use of concentric gas flow around the centered bio-oil injection line. In this design the coking was be controlled by adjusting the gas flow rates and injection temperature of the gas to keep the internal bio-oil line below coking temperature of 100^{o}C. A second water/steam line was added separately from the bio-oil and oxygen nozzle to prevent the system from over heating.

Another challenge that appeared during the gasifier construction that made us deviate from the original design was the inability to incorporate electrical external heaters that were supposed to provide adiabatic reaction conditions. The gasifier was redesigned to operate without heaters, controlling the temperatures of the reaction through highly insulated walls. In order to produce enough thermal energy to overcome heat loss at the desired reaction temperature, either the equivalence ratio had to be increased or the process flow rate needed to be increased. It was decided to increase the flow rate from 600 mL hr^{-1} to 1200 mL hr^{-1} while maintaining an equivalence ratio of 0.25. **Figure 5** shows the relationship between the energy

available in gasification at a flow rate of 1200 mL hr^{-1} verses the heat loss through a 5 inch diameter nominal pipe size by 40 inch long pressurized wall. As the temperature of the reaction was increased, the energy loss through the pressure vessel increased. Likewise as the temperature of the reaction increased the energy generation from gasification reduced. Therefore, the point where the two curves crossed was the optimal the operating temperature. This analysis indicated that the reactor could be run without external heat addition to temperatures as high as 950°C. This model was designed in 2D heat transfer to supply preliminary results and does not account for the energy losses through the flanges on the ends of the reactor.

Figure 4. Assembly of the test rig to be used for bio-oil gasification study at atmospheric pressure.

The reactor was designed in four major parts: the injection flange (see above), gasifier, quench and the bottom flange as is illustrated as a 3D model and cross-sectional view in **Figure 6**. The injection flange will not only house the injection nozzle but also a multipoint thermocouple to monitor process temperature, the steam injection tube to regulate reaction temperature, and two high pressure electrical studs to provide an ignition source for start up. The gasifier has three layers consisting of an inner silicon carbide tube to contain the gasification reaction, insulation to shield the pressure vessel from the reaction heat, and the outer stainless steel pressure vessel to maintain the vessels integrity. The stainless steel quench vessel will contain multiple water spray nozzles to quench the syngas to nearly room temperature before exiting the quench vessel. Quenching the gas provided two advantages: it eliminated the need for a high temperature pressure control valve for the exiting syngas line and it removed solid particles that remained in the gas stream along with any ammonia formed in the gasification process. The quench will also collect the excess liquid water in the bottom of the vessel to be drained through the bottom flange. Not only did the bottom flange extract the excess water from the quench vessel but also contained fittings for the water supply lines and additional ports for thermocouples to monitor the quench vessel temperatures.

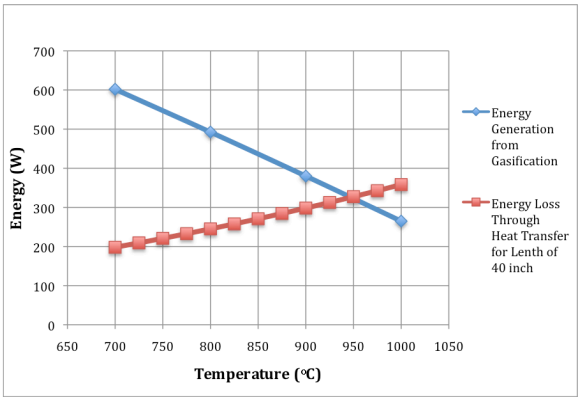

Figure 5: Available energy in gasification vs. energy loss due to heat transfer from the pressure vessel

Designing the reactor system was followed up with building a reactor frame and incorporating a reactor control system. The bio-oil reactor was near completion at the end of

the 10th quarter, a digital picture of the entire reactor is shown in **Figure 7**. The progress of building the bio-oil reactor and the follow-up shake-down trials were hampered due to a

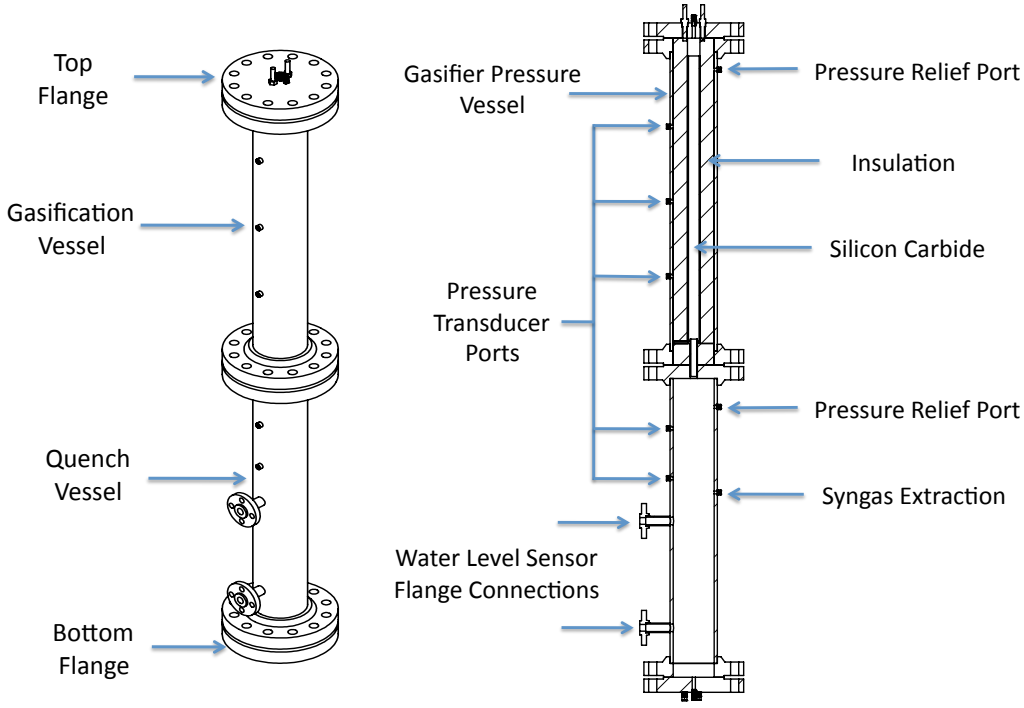

Figure 6. 3D model and cross-section view of the bio-oil reactor assembly

backordered heating system mainly because the main heater burned out because it was operating outside the manufacturer's specified parameters. While waiting for this heater the subsystems of the bio-oil reactor were tested to ensure each subsystem operated independently of the full reactor. This increased reliability and reduced the time in identifying and fixing problems that invariable appear upon start up.

Figure 7. Progress of bio-oil reactor at the end of Quarter

When the bio-oil reactor construction was completed, shakedown trials commenced. The challenges that appeared during the shake-down trials including determining mass balances and inability to fully quench the steam were addressed by adding a micro-GC and replacing a HPLC pump,

respectively. Methanol was chosen as the surrogate feed for the initial shakedown trials. During the 14th quarter the first trial runs with bio-oil were completed with bio-oil produced from pine. As shown in **Figure 8**, the syngas produced from bio-oil was unable to reach steady state before the available fuel was exhausted. Examination of the system showed that a large amount of residue was produced and collected in the quench and exit lines. This residue caused an increase in pressure throughout the system and also clogged the water nozzles in the quench vessel. Therefore, modifications where made to the quench vessel to increase its efficiency and reduce the chance of clogging. Additionally, it was hypothesized that the residue was a result of unreacted bio-oil passing through the gasifier due to heat transfer limitations or insufficient residence times within the

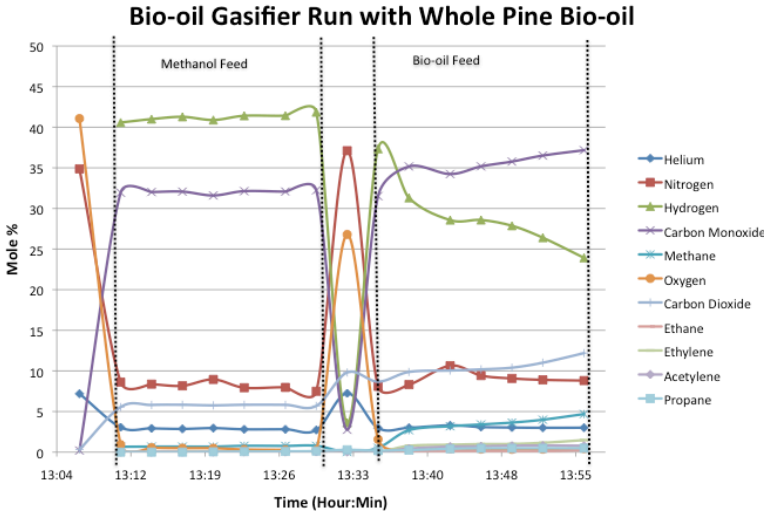

Figure 8: Syngas composition data using a whole pine bio-oil at a flow rate of 20 mL min^{-1}

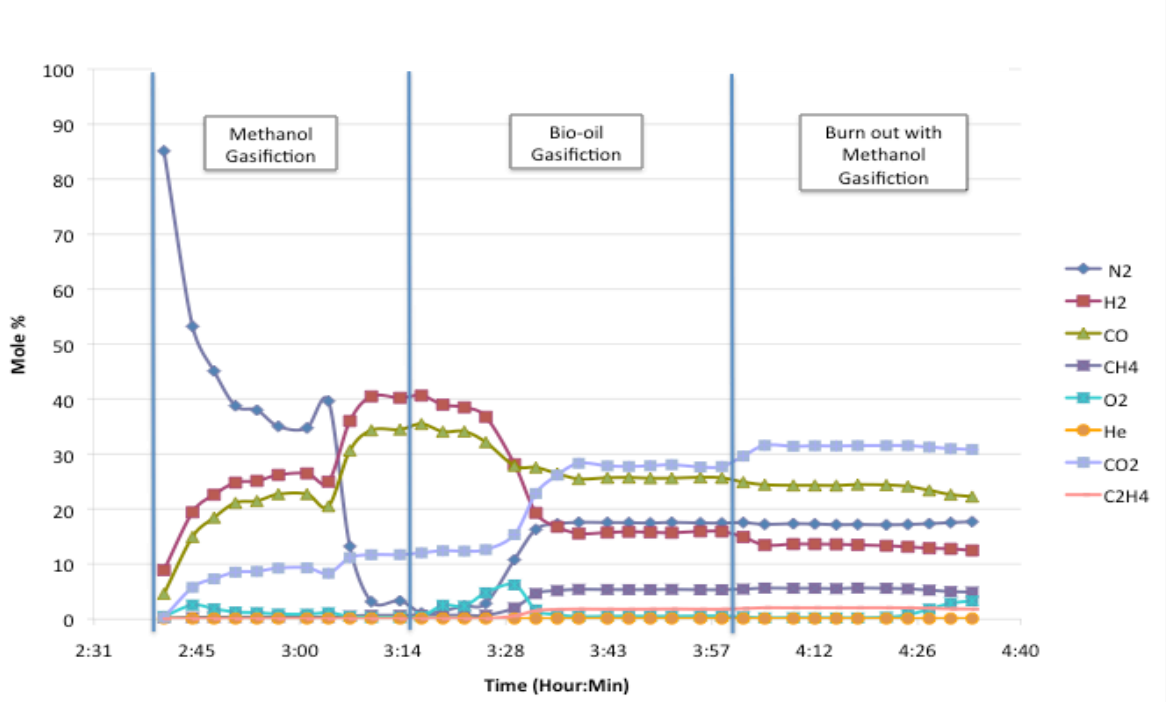

Figure 9: Syngas composition data produced at a flow rate 10 mL min^{-1} of bio-oil

reactor. To address this issue, the flow rate of the bio-oil was decreased. Two more bio-oil

gasification runs were completed. Both runs were operated at 10 mL min^{-1} of bio-oil. Temperatures were held at 900°C and pressure was maintained at 5 psi. The second run was successful in providing steady state data for bio-oil gasification at 5 psi and 900°C. As seen in **Figure 9**, the syngas produced from bio-oil at steady state contains approximately 16% hydrogen and 25% carbon monoxide.

Objectives set out by CCAT were to design and synthesize robust catalysts to convert bio-oil derived syngas to valuable products with a focus on developing C_2-oxygenates. The CCAT section of the project started by synthesizing several grams of rhodium supported on mesoporous silica nanoparticle (Rh-MSN) catalysts. We initially looked at the product yield of the syngas to C_2-oxygenate reaction with our microtubular reactor (flow diagram of the microtubular reactor is shown in **Figure 10**) with a H_2:CO stream (2:1). Concurrently with the catalyst synthesis and testing activities, new catalysts were characterized by a series of methods including solid-state NMR.

Table 3. Thermochemical microtubular reactor data of 2%Rh-MSN

	Temperature (°C)	CO conversion (%)	Carbon selectivity (mole %)				Carbon balance (%)
			Methane	CO_2	MeOH	EtOH	
1	250	1.1	53.3	~	25.3	21.2	86.8
2	280	2.3	58.7	6.4	34.9	~	98.2
3	290	4.4	61.8	4.5	18.9	16.8	100
4	300	10.9	51.7	6.5	20.8	21	72.2
5*	300	10.0	58.9	3.5	11.8	26	75.3

The first goal of the catalyst synthesis was to identify the optimal catalyst (Rh) loading on the MSN. Knowing that limited Rh could be loaded on to MSN and still maintain the pore structure and integrity (robustness was an important characterization of this catalyst) we synthesized three supported catalysts with different Rh loading (1.5, 2.0 and 2.5 wt %). We discovered that 2 wt.% Rh loading for this particular system was optimal and decided to focus on this catalyst. The first reactor variable that we tackled was temperature. The results from 2%Rh-MSN at different temperatures are described in **Table 3**. Interestingly, in the microtubular reactor we observed a significant temperature dependence on some product yields. As the temperature decreased the CO conversion decreased drastically. Higher temperatures led to a greater selectivity for ethanol over methanol, but increased methane production (**Figure 11**).

In order to incorporate the Rh on the MSN we attached a phosphine ligand group that coordinates directly to the Rh. We used solid-state NMR techniques to determine if the ligands were attached and to quantify the loading. Dr. Marek Pruski's research group obtained ^{29}Si cross polarization magic angle spin (CPMAS) experiment results to determine that phosphine

functionalization on the surface of the Rh-MSN catalyst did occur (**Figure 12**). Represented in the spectra are silicon sites of the types Q, T and M. The Q sites form the framework of the MSNs, with the wall core comprised of Q^4-type silicon atoms ($(SiO)_4Si$) and the surface containing Q^2 ($(SiO)_2Si(OH)_2$) and Q^3 ($(SiO)_3Si(OH)$) sites. The resonances representing Q^4, Q^3 and Q^2 sites are typically found near 110, 100, and 90 ppm, respectively. The sites denoted as T^2 and T^3, observed at approximately 58 and 68 ppm, are assigned to $(SiO)_2Si(R^0)R$ and $(SiO)_3SiR$ functionalities, where R represents the attached functional groups and R^0 ¼ OC_2H_5 or OH.

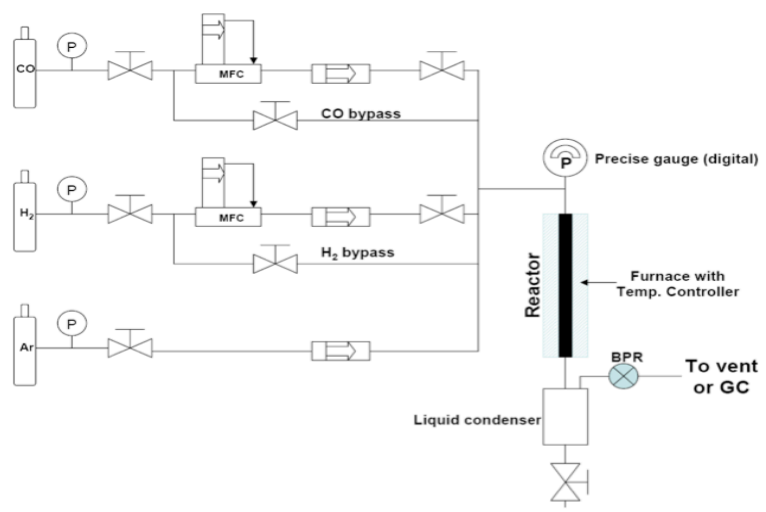

Figure 10. Flow diagram of a microtubular reactor

The presence of T sites indicates that functionalization of the MSN surfaces has indeed occurred. The M sites ((SiO-Si-$(CH_3)_3$) are observed at around 13 ppm, in agreement with earlier reports. These sites result from silylation (‘‘capping’’), a process by which surface hydroxyl hydrogens are substituted by trimethylsilyl groups. The relative concentrations of silicon sites in the RhP-MSN were found via deconvolution and integration of the resonances in the ^{29}Si DPMAS spectrum of **Figure 12c-12d**. Due to slow spin-lattice relaxation of ^{29}Si nuclei, the DPMAS experiment required more experimental time but provided relative peak intensities that are not distorted by the ^{1}H-^{29}Si CP process. An overall T site concentration of 3.7(±0.5)% was determined, which correlates well with the result obtained from EDX measurements of the same sample (3.8%). Also, the NMR specialists have begun to measure the phosphine ligands using ^{31}P CPMAS NMR techniques. This is a method to determine the oxidation state of the phosphorus when it is bound to the surface of the MSN.

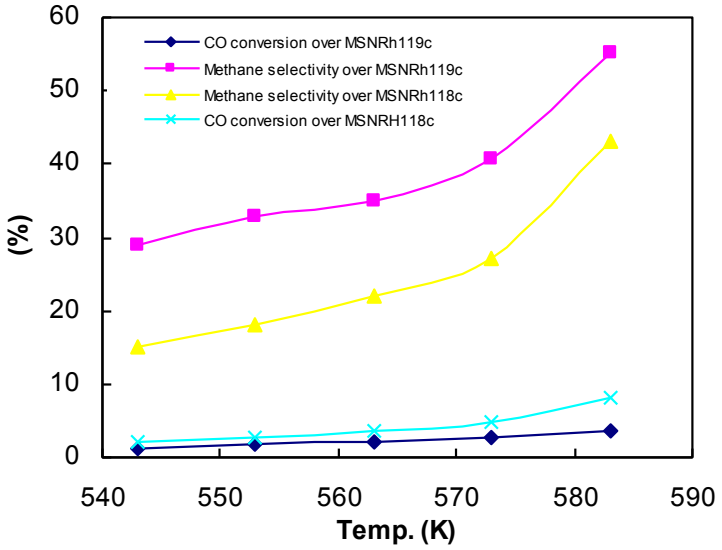

Figure 11. Repeated cycles of 2%RhMSN, observe the increased methane production over repeated

The optimal method to incorporate the Rh on the MSN was also a variable we explored during this project. The method described up to this point is a coordination of Rh to phosphine ligands covalently grafted to MSN materials followed by thermal treatments to sinter and form Rh nanoparticles on the MSN surface. Another method was to pre-synthesize Rh nanoparticles (Rh NPs) and incorporate them into the MSN via *in situ* methods (during the synthesis of the mesoporous silica). We initially compared the oxidation of the Rh NP before and after incorporating it into the MSN via X-ray photoelectron spectroscopy (XPS), an example of data is shown in **Figure 13**. We discovered that the Rh NP were oxidized to Rh_2O_3 upon incorporation and calcination but we were able to reduce the Rh back to Rh(0) by thermal treatment with H_2 (this was done *in* situ in the microtubular reactor).

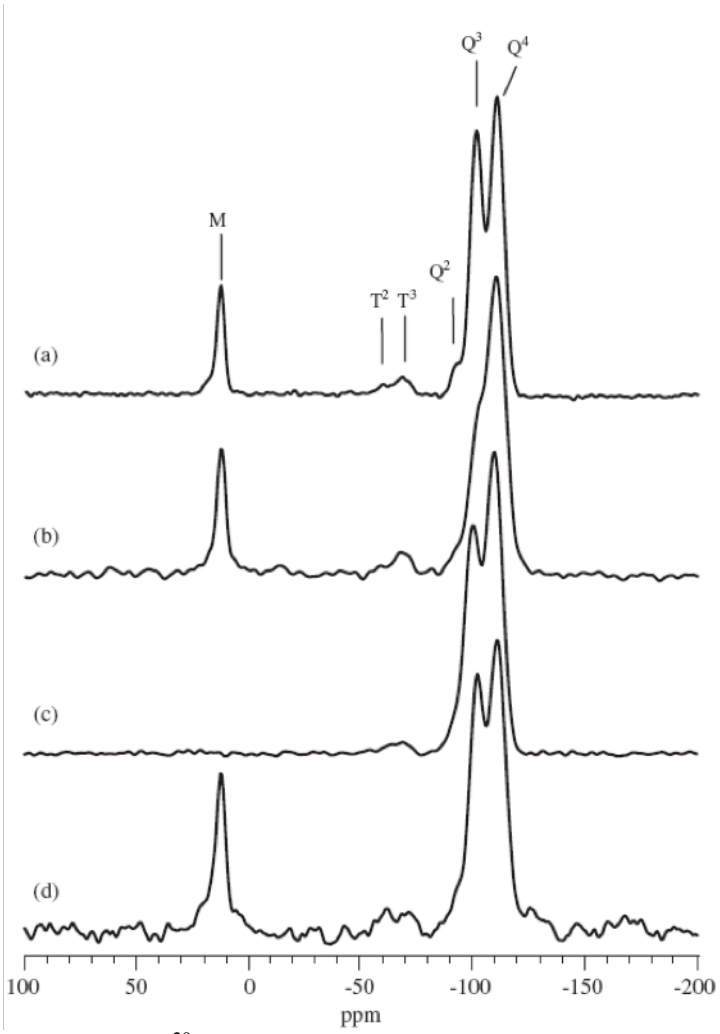

Figure 12. ^{29}Si CP/MAS NMR spectra of mesoporous silica nanoparticles functionalized with rhodium-phosphine ligands: a) unreacted catalyst (RhP-MSN) and b) catalyst reacted with syngas (RhP-MSN).

We also characterized the catalysts via transmission electron microscopy (TEM) and scanning transmission electron microscopy (STEM) (**Figure 14**). This method allowed us to visualize the Rh on the silica support, both before and after the catalysts were exposed to the syngas reactor conditions. Clearly the Rh NP that are incorporated into the support via in situ methods has a better stability as the Rh NPs did not appear to grow significantly under syngas reactor conditions.

In addition to supporting the active catalyst (Rh) on mesoporous silica we investigated support on ordered mesoporous carbon (OMC) materials. We successfully incorporated Rh on OMC as is shown in the TEM and STEM images in **Figure 14** and achieved uniform Rh nanoparticle distribution. We oxidized the OMC surface to form carboxylic groups that coordinate to the Rh, nitrogen sorption analyses data from OMC supported Rh catalyst with Mn promoter is outlined in **Table 4**. The catalytic performance of Rh-Mn/OMC was impressive from a selectivity viewpoint. The selectivity for C_2-oxygenates over methanol is 7:1 all while limiting the amount of CO, CO_2, and CH_4 that formed. All details are described in **Table 5** and **6**. Analysis of the Rh-Mn/OMC catalysts before and after exposure to the syngas

reactor conditions (conditions shown in **Table 7**) via electron microscopy showed good stability (**Figure 15**).

Further characterization of the Rh-Mn/OMC materials were completed with XPS exploring changes in the metals during actual reaction. **Table 8** shows the binding energies of Rh and Mn before and after the reaction. We discovered that Mn existed in the Mn^{2+} or higher valence states (Mn^{3+} and Mn^{4+}) before and after reduction. Mn^{2+} was unlikely to be reduced to metallic state and could influence the selectivity effectively with its high valence states as a promoter during CO hydrogenation. Additionally, we analyzed the surface properties of Rh-Mn/OMC via nitrogen sorption and determined that after exposing the catalyst to the syngas reaction conditions for 24 hours decreased the surface area, possibly due to pore collapse or growth in the metal nanoparticles (**Figure 16**).

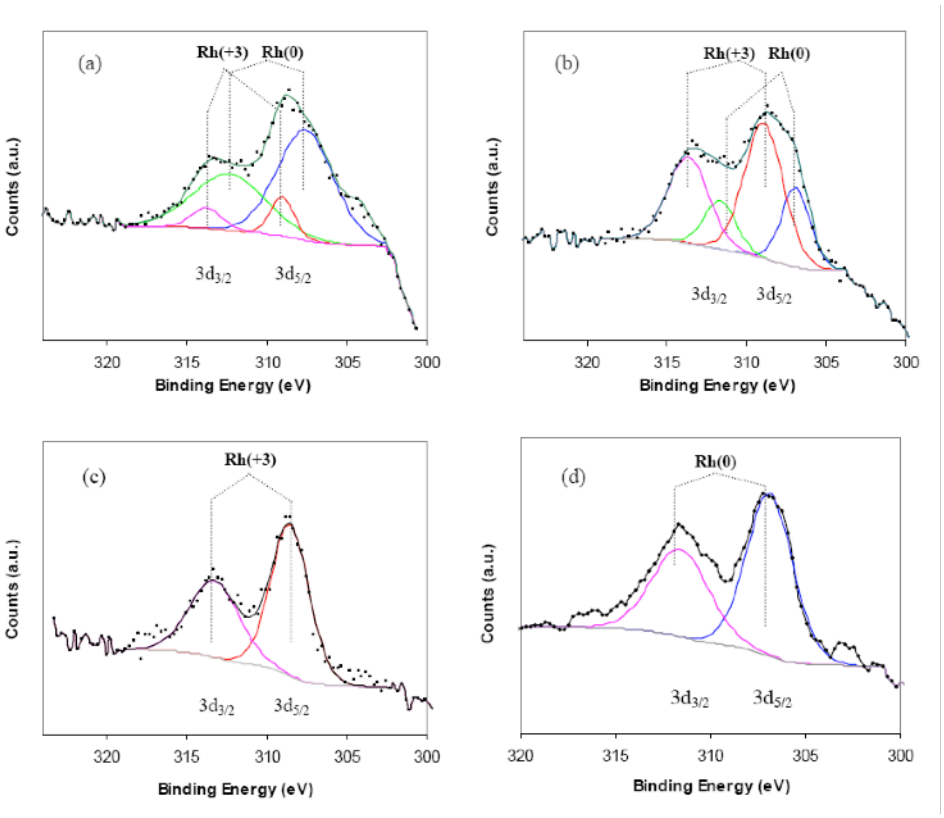

Figure 13. XPS of RhNPs (a) and MSNRhNPs (b) before calcination, (c) after calcination, (d) after reaction.

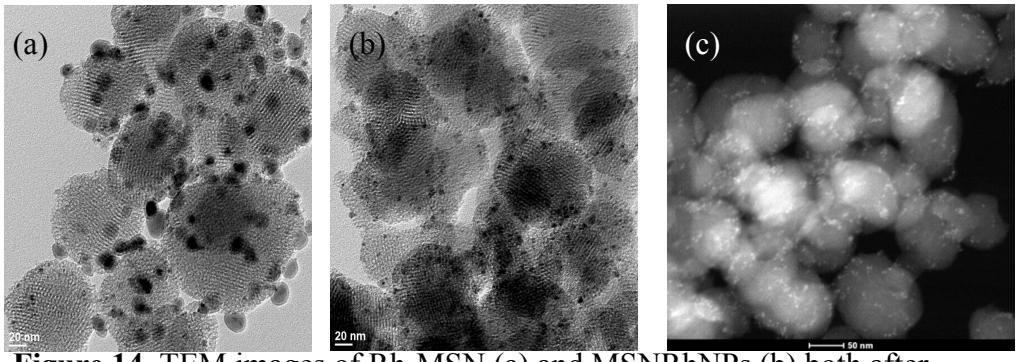

Figure 14. TEM images of Rh-MSN (a) and MSNRhNPs (b) both after reaction at 300 ^{o}C for 24h. STEM image of MSNRhNPs after synthesis (c).

We wanted to identify optimal earth abundant promoters for this reaction. We studied

Table 4. Structural properties of surface-functionalized OMCs[a]

Samples	S_{BET} (m^2g^{-1})	W_{BJH} (nm)	V_p (cm^3g^{-1})
OMC	1874	2.9	1.32
COOH-OMC	1567	2.3	0.97
Rh-Mn/OMC	1356	2.8	0.88
Rh-Mn/OMC (after reaction)	1132	<1.8	0.71

[a]: S_{BET} stand for surface area; W_{BJH} stand for pore diameter; V_p stand for total pore voume

manganese initially because there was substantial evidence in the literature that Mn acted as a strong promoter for alcohol in syngas upgrading. In order to compare catalysts with different promotion rapidly we focused on measuring the conversion of CO. We discovered that Rh-

Table 5. The catalytic performance and the selectivity of products of Rh-Mn/OMCs

Task	Temperature (^oC)	CO Conv. (%)	Selectivity (C %)[a]				
			CH_4	CO_2	MeOH	EtOH	C_{2+} Oxy[b]
1	280	8.45	7.97	15.88	14.67	38.74	22.74
2	300	14.61	14.09	15.73	8.62	34.38	27.17
3	310	33.21	9.3	15.53	6.22	40.63	28.32
4	320	43.26	10.12	14.74	6.79	39.53	28.82

[a]: Product selectivities are reported in terms of carbon efficiencies which is defined as:
Carbon efficiency = n_iC_i / $\sum$ (n_iC_i), where n_i is the number of carbon atoms and C_i is the molar concentration of the carbon-containing products.
[b]: Oxygenates with 2 or more carbons except ethanol (acetaldehyde, acetone, *i*-propanol, n-propanol)

MSN promoted by Fe and K converted the greatest amount of CO (17.4 %) while Co promoted Rh-MSN only converted 8.6% (**Table 9**). We used silica as the support for this study because we had more experience with the synthesis of mesoporous silica than mesoporous carbon.

Both aspects of this project were successful individually, CSET was able to make syngas from a switchgrass feedstock and the CCAT team synthesized, characterized, and tested Rh

Table 6. Catalytic performance of Rh-Mn/OMC on the microtubular reactor

	Gas Selectivity					Liquid products		
Temp (°C)	CH_4 (wt%)	CO_2 (wt%)	Ethane (wt%)	Total (wt%)	CO conv. (%)	MeOH (wt%)	EtOH (wt%)	$n_{MeOH}/(n_{EtOH+}n_{AcH})$
291	7.97	15.88	-	23.85	8.45	0.24	0.46	0.68
301	16.37	24.07	-	40.44	12.65	0.17	0.53	0.41
311	14.09	15.73	-	29.82	14.61	0.16	0.46	0.45
321	9.3	15.53	-	24.83	33.21	0.30	1.41	0.29
331	10.12	14.74	-	24.86	43.26	0.69	2.88	0.32
351	15.94	13.57	-	29.51	79.62	0.93	4.12	0.31

catalysts supported on mesoporous silica and mesoporous carbon for the targeted production of ethanol from syngas. The final goal of this project, combining the efforts to produce ethanol from syngas derived from switchgrass was thus far not complete. We were successful in constructing and troubleshooting a new bio-oil reactor that targeted CO and H_2 production. Substantial data was recorded on the production of Rh supported catalysts including

Table 7. Different reaction conditions on Rh-Mn/OMC catalyst conditions in a fixed bed reactor

Temp. (˚C)	Total Flow (ml min^{-1})	Hydrogen (%)	CO (%)	H_2/CO	He (%)
300[1]	310	57.66	33.46	1.72	3.61
300	155	N/A	N/A	N/A	N/A
300	155	N/A	N/A	N/A	N/A
300	620	54.81	30.80	1.78	3.32
300	465	58.58	30.53	1.91	3.31
300[2]	310	56.36	33.80	1.69	3.65
325	310	58.64	34.30	1.71	3.64
275	310	58.14	34.34	1.69	3.66

technically challenging solid-state NMR and XPS. The nature of the active metal catalysts was related to the product yields.

Table 8. Binding energies of Rh-Mn/OMC before and after reaction

Sample	Testing conditions	Binding energies (eV)	
		Mn2$p_{3/2}$	Rh3$d_{5/2}$
Rh-Mn/OMC	Before reduction	641.0	308.3
	After reduction	641.8	307.0

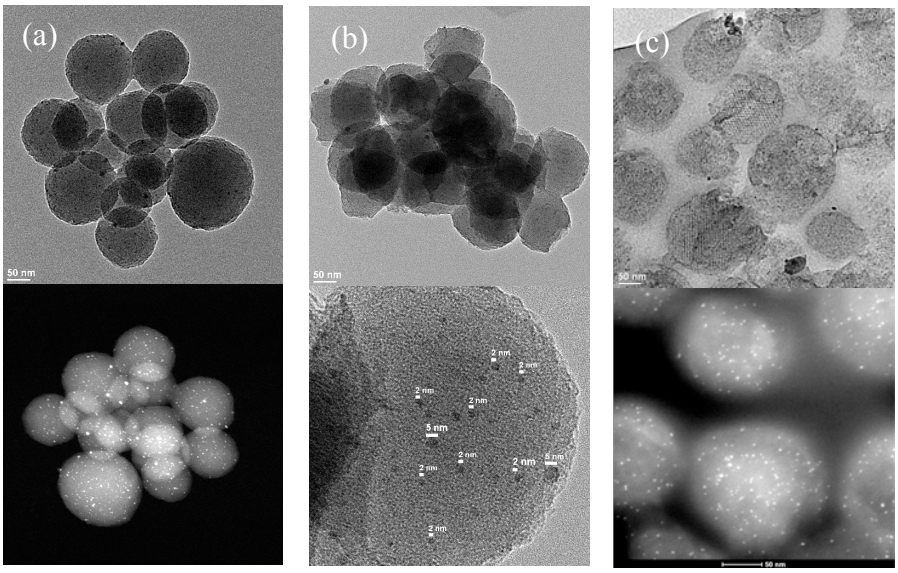

Figure 15. TEM and STEM micrographs of Rh/OMC (a); Rh/OMC(rxn) (b); ultramicrotomed Rh/OMC (rxn) (c)

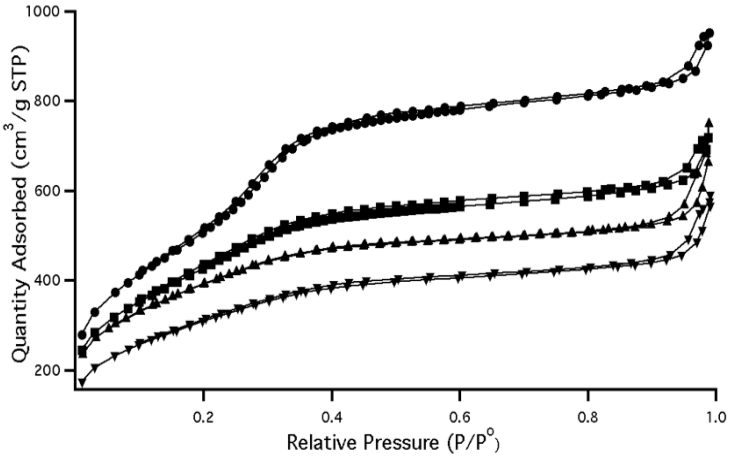

Figure 16. BET isotherms of surface functionalized OMC, -●- OMC; -■- COOH-OMC; -▲- Rh-Mn/OMC; -▼- Rh-Mn/OMC (rxn)

Next steps

The next steps for this research should look into both the conversion of biomass to syn gas (CSET contributions) and the subsequent targeted C_{2+} oxygenate synthesis (CCAT contribution). Currently four different research directions come to mind to grow this field: (1) designing reactors that can be used with multiple catalysts in a series platform, (2) investigating promotion effects of metals other than Mn, (3) exploring the effects of minerals typically found in biomass on the syn gas production, and (4) experimentally testing theoretical results discovered on faceted Rh nanoparticles on the formation of C_2 oxygenates. These ideas for future research programs are outlined below.

Designing in series reactors for selective product formation. We demonstrated that our catalyst could target C_{2+} oxygenates; however, this still leaves a considerable amount of different products including acetic acid, acetaldehyde, ethanol and larger carbon molecules as minor products. A microtubular reactor could be retrofitted for additional catalyst plugs to follow the Rh/MSN catalyst to upgrade these products to achieve a single product stream, i.e. both acetic acid and acetaldehyde could be reduced over a platinum catalyst. Decreasing the product stream to fewer molecules, with the ultimate goal to get it down to ethanol only, would decrease necessary downstream upgrading and overall cost savings.

Investigating promotion effects of metals other than manganese. While manganese showed positive promotion for C_{2+} oxygenates when incorporated in the MSN with Rh, the scope of our project did not cover exploring other promoting metals. Recent evidence has shown that metals including iron, cerium, and molybdenum promote the formation of C_{2+} oxygenates when incorporated with Rh.[1-3] However, it is unknown how these metals would compare to Mn, not only in the level of promotion but in the incorporation in the mesoporous supports. There are two variables at play with this system, how well do the metals promote the selective formation of C_{2+} oxygenates with Rh but, additionally, how well do the metals incorporate in the mesoporous silica and carbon supports in close proximity to the active metal. We recently demonstrated the ability to synthesize mesoporous silica with a homogeneous distribution of Mo in the silica and others have shown the ability to do this with Fe and Ce, but without another metal (i.e. Rh),[4] could the effect of the promotion be improved with a metal that would distribute in the support more readily?

Exploring mineral effects on conversion of biomass to syn gas. In addition to future directions for catalyst development there are several variables in the biomass conversion that need to be addressed. One important variable is the identity and concentration of inorganic minerals on the formation of syn gas from biomass. Typically, minerals lead to ash during pyrolysis and gasification processes of biomass, but the amount of ash formed is a consequence of what inorganic elements and the quantity in the biomass. A study has been published on potassium and phosphorous effects on gasification of biomass but this is a single study,[5] there are many other inorganic candidates (and quantities there of) that should be investigated. As different pyrolysis reactors are designed inorganics could have unique effects on product formation.

Experimentally testing faceted Rh nanoparticles on the formation of C_{2+} oxygenates. Recent theoretical evidence indicate that different faces of faceted Rh nanoparticles of unique reactivity, shown by several groups using density functional theory.[6-7] In this case, the Rh[211] face showed a 6x improved selectivity for acetaldehyde over the Rh[111] face. With new synthetic capabilities to control the faceted growth of metals and metal oxides new experiments can be designed to test these computational modeling studies.[8-9]

In additional to these studies, there is a significant research area focusing on the activity of sulfide cobalt-molybdenum (S-CoMo) catalysts for syn gas conversion to C_{2+} oxygenates. Of course a big advantage of this catalyst is the earth abundance of the active metals (Co and Mo) compared to Rh but one disadvantage is the need to frequently feed in sulfur to replace leached sulfur from the catalyst leading to additional upgrading steps (sulfur removal) in the product stream. Careful comparisons of these two systems from an experimental, technoeconomic analysis, and life cycle assessment viewpoint would be beneficial.
These represent a few directions research in ethanol from biomass via syn gas could go, there are many other variables that could be manipulated and studied to optimize the production of drop-in transportation fuels

1. Liu, W.; Wang, S.; Sun, T.; Wang, S., The Promoting Effect of Fe Doping on Rh/CeO_2 for the Ethanol Synthesis. *Catalysis Letters* **2015,** *145* (9), 1741-1749.
2. Mao, W.; Su, J.; Zhang, Z.; Xu, X.-C.; Fu, D.; Dai, W.; Xu, J.; Zhou, X.; Han, Y.-F., A mechanistic basis for the effects of Mn loading on C_{2+} oxygenates synthesis directly from syngas over Rh-MnOx/SiO2 catalysts. *Chemical Engineering Science* **2015,** *135*, 301-311.
3. Liu, W.; Wang, S.; Wang, S., Effect of impregnation sequence of Ce promoter on the microstructure and performance of Ce-promoted $Rh-Fe/SiO_2$ for the ethanol synthesis. *Applied Catalysis, A: General* **2016,** *510*, 227-232.
4. Budhi, S.; Peeraphatdit, C.; Pylypenko, S.; Nguyen, V. H. T.; Smith, E. A.; Trewyn, B. G., Enhanced metal loading in SBA-15-type catalysts facilitated by salt addition: Synthesis, characterization and catalytic epoxide alcoholysis activity of molybdenum incorporated porous silica. *Appl Catal a-Gen* **2014,** *475*, 469-476.
5. Chakrabarti, R.; Schmidt, L. D., Role of Potassium and Phosphorus in Catalytic Partial Oxidation in Short Contact Time Reactors. *Energy & Fuels* **2015,** *29* (12), 8102-8109.
6. Yang, N.; Medford, A. J.; Liu, X.; Studt, F.; Bligaard, T.; Bent, S. F.; Norskov, J. K., Intrinsic Selectivity and Structure Sensitivity of Rhodium Catalysts for C_{2+} Oxygenate Production. *J Am Chem Soc* **2016,** *138* (11), 3705-14.
7. Wang, J.; Liu, Z.; Zhang, R.; Wang, B., Ethanol Synthesis from Syngas on the Stepped Rh(211) Surface: Effect of Surface Structure and Composition. *Journal of Physical Chemistry C* **2014,** *118* (39), 22691-22701.
8. Khi, N. T.; Park, J.; Baik, H.; Lee, H.; Sohn, J.-H.; Lee, K., Facet-controlled {100}Rh-Pt and {100}Pt-Pt dendritic nanostructures by transferring the {100} facet nature of the core nanocube to the branch nanocubes. *Nanoscale* **2015,** *7* (9), 3941-3946.
9. Li, Z.; Ciobanu, C. V.; Hu, J.; Palomares-Baez, J.-P.; Rodriguez-Lopez, J.-L.; Richards, R., Experimental and DFT studies of gold nanoparticles supported on MgO(111) nano-sheets and their catalytic activity. *Physical Chemistry Chemical Physics* **2011,** *13* (7), 2582-2589.

Products:

A. **Thesis Chapters:**

A solid-state NMR investigation of the structure of mesoporous silica nanoparticle supported rhodium catalysts

Jennifer L. Rapp [a], Yulin Huang [c], Michael Natella [b], Yang Cai [c], Victor S.-Y. Lin [a,c], Marek Pruski [a,c,]
[a] US DOE Ames Laboratory, Iowa State University, Ames, IA 50011, USA
[b] Ecole Nationale Superieure des Ingenieurs en Arts Chimiques et Technologiques, Toulouse 31077, France
[c] Department of Chemistry, Iowa State University, Ames, IA 50011, USA

Chapter 4. M-Modified and Well-defined Rh nanoparticles Supported on Mesoporous Silica Nanoparticles: Highly-selective Synthesis of Ethanol from Syngas
Yulin Huang,[1] Weihua Deng,[2] Enruo Guo,[1] Senniang Chen,[1] Po-Wen Chung,[1] Brian G. Trewyn,[1] Victor S.-Y. Lin[1],*
1. Department of Chemistry and Ames Laboratory-U.S. Department of Energy, Iowa State University, Ames, IA 50011, 2. Center for Sustainable Environmental Technologies, Iowa State University, Ames, IA 5001
Chapter 4. Ordered Mesoporous Carbon Nanoparticles as a Support for the Conversion of Syngas to Alcohol
Po-Wen Chung, Tae-Wan Kim, Yulin Huang, Weihua Deng, Robert Brown, Victor S.-Y. Lin*

B. Poster Presentations

Creager, N., Whitmer, L., Kong, S-C, Brown, R.C. *High Pressure, Oxygen Blown, Entrained Flow Gasification of Bio-oil*, **International Conference on Thermochemical Conversion of Biomass**, September 3-6, 2013, Chicago, IL

Yulin Huang, Nick Creager, Ryan Smith, Robert C. Brown, Brian G. Trewyn, and Victor S.-Y. Lin, *Catalytic Production of Ethanol from Biomass-Derived Synthesis Gas*, **DOE EERE Thermochemical Technical Review**, February 2011